Available online at www.sciencedirect.com
SCIENCE DIRECT®
International Journal of Heat and Mass Transfer 47 (2004) 1685–1700
International Journal of HEAT and MASS TRANSFER
www.elsevier.com/locate/ijhmt

Transient natural convection heat transfer of fluids with variable viscosity between concentric and vertically eccentric spheres

Horng Wen Wu [a,*], Wen Ching Tsai [a], Huann-Ming Chou [b]

[a] Department of Systems and Naval Mechatronic Engineering, National Cheng Kung University, Tainan 701, Taiwan, ROC
[b] Department of Mechanical Engineering, Kun Shan University of Technology, Tainan 710, Taiwan, ROC

Received 29 May 2003; received in revised form 25 October 2003

Abstract

The transient natural convection has been analyzed for the temperature dependent viscosity of fluids in spherical annulus and between two vertically eccentric spheres. Using the modified Sorenson's method to generate the grid line can get the grid system with orthogonality along all boundaries. The grid system goes along with weighting function scheme to discretize the general governing equation. Numerical solutions were obtained for Rayleigh numbers (5.0×10^3–6.5×10^4) at a radius ratio of 2.0 with the dimensionless vertical eccentricity of the outer sphere (0–$\pm$0.65) for variable viscosity fluids at different Prandtl numbers (158, 405 and 720). The results of this analysis show that heat and flow patterns vary with the Rayleigh number and the eccentricity; besides, the effect of variable viscosity is investigated. The present calculations applied to constant viscosity are compared with the results of other papers, and these comparison results are agreeable.

1. Introduction

Natural convection in enclosures finds many practical applications in the many diverse fields of present engineering practice, such as the cooling of the passive cooling of advanced nuclear reactors, the solar energy collector, gyroscope, geophysical fields, and the thermal storage systems [1]. It is important in these applications to realize flow field and heat transfer in enclosures considering the effect of local buoyancy.

For the environment with large temperature difference and the fluid with high Prandtl number, the change of physical properties is affected most by the viscosity. Therefore, the consideration of influence from the temperature dependent viscosity of fluid in enclosures is necessary. Horne and O'Sullivan [2] investigated the effect of temperature dependent viscosity and thermal expansion coefficient on convection in a porous medium heated and found the critical Rayleigh number decreased 31%. Wazzan et al. [3,4] studied the stability of water flow over heated and cooled flat planes with variable viscosity fluids. Jang and Mollendorf [5] found the effect of variable viscosity tending to stabilize a vertical natural convection boundary layer. Chou et al. [6] presented that the effect of variable viscosity makes temperature gradient of fluid larger and this gradient increases as Prandtl number increases.

The problem of natural convection in a spherical annulus and between two vertically eccentric spheres is more intricate than in other configurations of enclosures to solve exactly due to complicated configurations. Mack and Hardee and others [7–13] had the related research for the mechanism of natural convection between concentric and vertically eccentric spheres or in horizontal eccentric annuli. The viscosity of working fluid is assumed to be constant in those papers and fluid patterns with lower Prandtl numbers were investigated.

* Corresponding author. Tel.: +886-6-274-7018; fax: +886-6-274-7019.
E-mail address: z7708033@email.ncku.edu.tw (H.W. Wu).

0017-9310/$ - see front matter © 2003 Elsevier Ltd. All rights reserved.
doi:10.1016/j.ijheatmasstransfer.2003.10.018

Nomenclature

C	coefficients used in Eq. (9)
D, E, F, G	parameters used in obtaining the glycerol–water solution viscosity
e	vertical eccentricity
f	dynamic viscosity ratio ($\mu(T)/\mu_m$)
g	local gravitation acceleration
J	Jacobian
L	annular gap ($\bar{r}_o - \bar{r}_i$)
m	exponential constants occurs in Eq. (9)
Nu	local Nusselt number (hL/k)
$\overline{Nu}$	averaged Nusselt number
P, Q	function used in coordinate transformation
Pr	Prandtl number ($\mu_m/\rho_m\alpha_m$)
Ra	Rayleigh number ($g\beta_m(\overline{T}_i - \overline{T}_o)L^3/\nu_m\alpha_m$)
R^*	ratio of outer and inner radius ratio, r_o/r_i
$\bar{r}$	radial coordinate
r	dimensionless radial coordinate ($\bar{r}/L$)
$\overline{T}$	temperature
T	dimensionless temperature ($(\overline{T} - \overline{T}_o)/(\overline{T}_i - \overline{T}_o)$)

Greek symbols

α	thermal diffusivity
β	thermal expansion coefficient
ε	dimensionless vertical eccentricity (e/L)
θ	polar angular coordinate
θ^*	polar angle at vortex center
φ	cone angular coordinate
α^*, β^*, γ^*	factor of coordinate transformation
ξ	transverse coordinate in transformed plane
η	longitudinal coordinate in transformed plane
μ	dynamic viscosity
ν	kinematic viscosity
ρ	fluid density
τ	dimensionless time ($t\alpha/L^2$)
$\bar{\psi}$	stream function
ψ	dimensionless stream function ($\bar{\psi}/\alpha L$)
$\bar{\omega}$	vorticity
ω	dimensionless vorticity ($\bar{\omega}L^2/\alpha$)
ϕ	variables occurs in coordinate transformation

Subscripts

i	inner
m	reference value
o	outer
max	maximum

The fluids with higher Prandtl numbers and with temperature dependent viscosity in a spherical annulus were not studied in the past so that the research is motivated in this paper.

Therefore, the objective of this paper is to investigate the transient natural convection of fluids with high Prandtl number and temperature dependent viscosity in a spherical annulus and between two vertically eccentric spheres. Effects of variable viscosity and eccentricity on the flow field, temperature distribution and heat transfer are discussed. The related equations between the averaged Nusselt numbers and Ra number are provided for various eccentricities and Prandtl numbers.

2. Mathematical analysis

Consider a spherical annulus and two vertically eccentric spheres filled with quiescent and viscous fluid as shown in Fig. 1. The fluid is glycerol–water solutions with solution concentrations 70%, 80% and 90%; corresponding to Prandtl numbers are 158, 405 and 720 for glycerol–water solutions as adopted by Chen and Pearlstein [14]. The related physical properties of glycerol–water solutions could be found from Segur [15] and Segur and Oberstar [16].

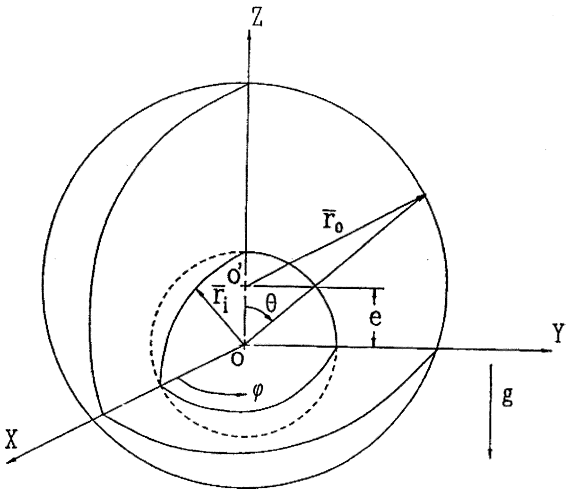

Fig. 1. Coordinate system for physical domain.

Initially, the fluid inside the enclosure is at uniform temperature and a quiescent state is assumed, while the inner sphere is suddenly changed to a higher temperature ($\overline{T}_i$) and outer sphere is maintained at lower temperature ($\overline{T}_o$). The eccentricity of two vertical spheres

is e. While the center of outer sphere is above that of inner sphere, e is positive. While the center of outer sphere is below that of inner sphere, e is negative. $\bar{\theta}$ is positive while it is clockwise. To formulate the problem, it is assumed that (1) fluid is Newtonian fluid, axisymmetric laminar and incompressible flows, (2) all fluid properties, are taken to be constant, except both the density in term of buoyancy with the assumption of Boussinesq and viscosity variation with temperature, (3) viscous dissipation is neglected; (4) radiation and compression effects are neglected.

A grid coordinate system is built by the way of the grid generation of controllably body-fitted elliptic partial differentiation in this paper. The coordinate (r,θ) of every point in a physical plane is transformed into a coordinate (ξ,η) in a calculation plane by coordinate transformation as shown in Fig. 2. In the process of coordinate transformation, the first and second partial derivatives are denoted in term of chain rule as

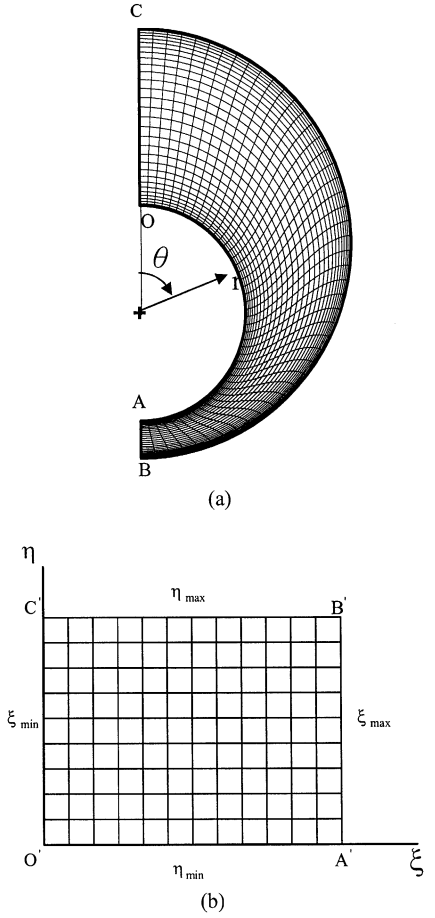

Fig. 2. The coordinate (r,θ) of every point in (a) physical plane transformed into a coordinate (ζ,η) in the (b) calculated plane.

$$\begin{bmatrix}\xi_r & \xi_\theta\\ \eta_r & \eta_\theta\end{bmatrix}=\frac{1}{J}\begin{bmatrix}\theta_\eta & -r_\eta\\ -\theta_\xi & r_\xi\end{bmatrix}$$

$$j=r_\xi\theta_\eta-r_\eta\theta_\xi$$

$$\frac{\partial\phi}{\partial r}=\frac{\partial\phi}{\partial\xi}\frac{\partial\xi}{\partial r}+\frac{\partial\phi}{\partial\eta}\frac{\partial\eta}{\partial r}$$

$$\frac{\partial\phi}{\partial\theta}=\frac{\partial\phi}{\partial\xi}\frac{\partial\xi}{\partial\theta}+\frac{\partial\phi}{\partial\eta}\frac{\partial\eta}{\partial\theta}$$

$$\begin{aligned}\frac{\partial^2\phi}{\partial r^2}&=\frac{\partial^2\phi}{\partial\xi^2}\left(\frac{\partial\xi}{\partial r}\right)^2+2\frac{\partial^2\phi}{\partial\xi\partial\eta}\frac{\partial\xi}{\partial r}\frac{\partial\eta}{\partial r}\\&\quad+\frac{\partial^2\phi}{\partial\eta^2}\left(\frac{\partial\eta}{\partial r}\right)^2+\frac{\partial\phi}{\partial\xi}\frac{\partial^2\xi}{\partial r^2}+\frac{\partial\phi}{\partial\eta}\frac{\partial^2\eta}{\partial r^2}\end{aligned}\tag{1}$$

$$\begin{aligned}\frac{\partial^2\phi}{\partial\theta^2}&=\frac{\partial^2\phi}{\partial\xi^2}\left(\frac{\partial\xi}{\partial\theta}\right)^2+2\frac{\partial^2\phi}{\partial\xi\partial\eta}\frac{\partial\xi}{\partial\theta}\frac{\partial\eta}{\partial r}\\&\quad+\frac{\partial^2\phi}{\partial\eta^2}\left(\frac{\partial\eta}{\partial\theta}\right)^2+\frac{\partial\phi}{\partial\xi}\frac{\partial^2\xi}{\partial\theta^2}+\frac{\partial\phi}{\partial\eta}\frac{\partial^2\eta}{\partial\theta^2}\end{aligned}$$

where ϕ is variable.

From above assumption and coordinate transformation, the governing equation of spherical coordinate system can be obtained.

Stream function equation:

$$\begin{aligned}&\omega r\sin\theta\\&=\frac{1}{J^2}\left(\alpha^*\frac{\partial^2\psi}{\partial\xi^2}-2\beta^*\frac{\partial^2\psi}{\partial\xi\partial\eta}+\gamma^*\frac{\partial^2\psi}{\partial\eta^2}\right)\\&\quad+\frac{\partial\psi}{\partial\xi}\left[P+\frac{1}{J}\left(\frac{\cot\theta}{r^2}r_\eta\right)\right]+\frac{\partial\psi}{\partial\eta}\left[Q-\frac{1}{J}\left(\frac{\cot\theta}{r^2}r_\xi\right)\right]\end{aligned}\tag{2}$$

Vorticity transport equation:

$$\begin{aligned}&\frac{\partial\omega}{\partial\tau}+\frac{1}{r^2\sin\theta}\frac{1}{J}\left[(A1)+\frac{\omega}{r}(B1)-\omega\cot\theta(B2)\right]\\&=f\cdot Pr\cdot\left\{\frac{1}{J^2}\left(\alpha^*\frac{\partial^2\omega}{\partial\xi^2}-2\beta^*\frac{\partial^2\omega}{\partial\xi\partial\eta}+\gamma^*\frac{\partial^2\omega}{\partial\eta^2}\right)\right.\\&\quad+\frac{\partial\omega}{\partial\xi}\left[P+\frac{1}{J}\left(\frac{2}{r}\theta_\eta-\frac{\cot\theta}{r^2}r_\eta\right)\right]\\&\quad\left.+\frac{\partial\omega}{\partial\eta}\left[Q-\frac{1}{J}\left(\frac{2}{r}\theta_\xi-\frac{\cot\theta}{r^2}r_\xi\right)\right]-\frac{\omega}{r^2\sin^2\theta}\right\}\\&\quad+2\cdot Pr\cdot\frac{1}{J^2}[A2]+Pr\cdot\frac{1}{J}\left[\frac{\partial f}{\partial\xi}\theta_\eta-\frac{\partial f}{\partial\eta}\theta_\xi\right]\\&\quad\times\left\{\frac{2}{r}\omega+\frac{2}{r^3\sin\theta}\frac{1}{J}(B2)-\frac{1}{r^2\sin\theta}\frac{1}{J^2}(B3)\right\}\\&\quad+Pr\cdot\frac{1}{J}\left[-\frac{\partial f}{\partial\xi}r_\eta+\frac{\partial f}{\partial\eta}r_\xi\right]\times\left\{\frac{\cot\theta}{r^2}\omega+\frac{2\cot\theta}{r^4\sin\theta}\frac{1}{J}(B2)\right.\end{aligned}$$

$$+\frac{6}{r^5\sin\theta}\frac{1}{J}(B1)-\frac{4}{r^4\sin\theta}\frac{1}{J^2}(B4)\Bigg\}$$
$$+Pr\cdot\frac{1}{J^2}\left[(C1)\frac{\partial^2 f}{\partial\xi^2}-2(C2)\frac{\partial^2 f}{\partial\xi\partial\eta}+(C3)\frac{\partial^2 f}{\partial\eta^2}\right.$$
$$\left.+(C4)\frac{\partial f}{\partial\xi}+(C5)\frac{\partial f}{\partial\eta}\right]\times\left\{-\omega-\frac{1}{r^2\sin\theta}\frac{1}{J}(B2)\right.$$
$$\left.+\frac{2}{r\sin\theta}\frac{1}{J^2}(B3)\right\}+Pr\cdot\frac{2}{r}\frac{1}{J^2}\left[(D1)\frac{\partial f}{\partial\xi}+(D2)\frac{\partial f}{\partial\eta}\right.$$
$$\left.+(D3)\frac{\partial^2 f}{\partial\xi\partial\eta}-(D4)\frac{\partial^2 f}{\partial\xi^2}-(D5)\frac{\partial^2 f}{\partial\eta^2}\right]$$
$$\times\left\{-\frac{\cot\theta}{r^2\sin\theta}\frac{1}{J}(B2)-\frac{3}{r^3\sin\theta}\frac{1}{J}(B1)\right.$$
$$\left.-\frac{2}{r^2\sin\theta}\frac{1}{J^2}(B4)\right\}$$
$$-Ra\cdot Pr\frac{1}{J}\left[\frac{\partial T}{\partial\xi}\left(\sin\theta\theta_\eta-\frac{\cos\theta}{r}r_\eta\right)\right.$$
$$\left.-\frac{\partial T}{\partial\eta}\left(\sin\theta\theta_\xi-\frac{\cos\theta}{r}r_\xi\right)\right] \tag{3}$$

$$A1=\frac{\partial\omega}{\partial\eta}\frac{\partial\psi}{\partial\xi}-\frac{\partial\omega}{\partial\xi}\frac{\partial\psi}{\partial\eta}$$
$$A2=\alpha^*\frac{\partial f}{\partial\xi}\frac{\partial\omega}{\partial\xi}+\gamma^*\frac{\partial f}{\partial\eta}\frac{\partial\omega}{\partial\eta}-\beta^*\frac{\partial f}{\partial\xi}\frac{\partial\omega}{\partial\eta}-\beta^*\frac{\partial f}{\partial\eta}\frac{\partial\omega}{\partial\xi}$$
$$B1=\frac{\partial\psi}{\partial\eta}\frac{\partial r}{\partial\xi}-\frac{\partial\psi}{\partial\xi}\frac{\partial r}{\partial\eta},\quad B2=\frac{\partial\psi}{\partial\xi}\frac{\partial\theta}{\partial\eta}-\frac{\partial\psi}{\partial\eta}\frac{\partial\theta}{\partial\xi}$$
$$B3=\frac{\partial^2\psi}{\partial\xi^2}\theta_\eta^2-2\frac{\partial^2\psi}{\partial\xi\partial\eta}\theta_\xi\theta_\eta+\frac{\partial^2\psi}{\partial\eta^2}\theta_\xi^2$$
$$+(\theta_{\xi\eta}\theta_\eta-\theta_{\eta\eta}\theta_\xi)\frac{\partial\psi}{\partial\xi}+(\theta_{\xi\eta}\theta_\xi-\theta_{\xi\xi}\theta_\eta)\frac{\partial\psi}{\partial\eta}$$
$$B4=\frac{\partial^2\psi}{\partial\xi^2}r_\eta\theta_\eta-\frac{\partial^2\psi}{\partial\xi\partial\eta}(r_\xi\theta_\eta+r_\eta\theta_\xi)+\frac{\partial^2\psi}{\partial\eta^2}r_\xi\theta_\xi$$
$$-(r_{\eta\eta}\theta_\xi-r_{\xi\eta}\theta_\eta)\frac{\partial\psi}{\partial\xi}-(r_{\xi\xi}\theta_\eta-r_{\xi\eta}\theta_\xi)\frac{\partial\psi}{\partial\eta}$$
$$C1=\theta_\eta^2-\frac{1}{r^2}r_\eta^2,\quad C2=\theta_\xi\theta_\eta-\frac{1}{r^2}r_\xi r_\eta$$
$$C3=\theta_\eta^2-\frac{1}{r^2}r_\xi^2$$
$$C4=\theta_{\xi\eta}\theta_\eta-\theta_{\eta\eta}\theta_\xi-\frac{1}{r^2}r_{\xi\eta}r_\eta+\frac{1}{r^2}r_{\eta\eta}r_\xi$$
$$C5=\theta_{\xi\eta}\theta_\xi-\theta_{\xi\xi}\theta_\eta-\frac{1}{r^2}r_{\xi\eta}r_\xi+\frac{1}{r^2}r_{\xi\xi}r_\eta$$
$$D1=r_{\eta\eta}\theta_\xi-r_{\xi\eta}\theta_\eta,\quad D2=r_{\xi\xi}\theta_\eta-r_{\xi\eta}\theta_\xi$$
$$D3=r_\xi\theta_\eta+r_\eta\theta_\xi,\quad D4=r_\eta\theta_\eta,\quad D5=r_\xi\theta_\xi$$
$$f=\mu(T^*)/\mu_m$$

where $\mu(T^*)$ uses the four-parameter form correlation of viscosity–temperature [14]:

$$\mu(T^*)=D\mathrm{e}^{\frac{E}{T^{*3}}+FT^*+\frac{G}{T^*}}$$

where four-parameters D, E, F and G are physical properties of glycerol–water solutions [15,16] obtained by method of the least square error.

$$\alpha^*=\theta_\eta^2+\frac{1}{r^2}r_\eta^2,\quad \beta^*=\theta_\eta\theta_\xi+\frac{1}{r^2}r_\eta r_\xi,\quad \gamma^*=\theta_\xi^2+\frac{1}{r^2}r_\xi^2,$$
$$P=\xi_{rr}+\frac{1}{r^2}\xi_{\theta\theta}$$
$$Q=\eta_{rr}+\frac{1}{r^2}\eta_{\theta\theta}$$
$$\alpha^* r_{\xi\xi}-2\beta^* r_{\xi\eta}+\gamma^* r_{\eta\eta}=-J^2(Pr_\xi+Qr_\eta)$$
$$\alpha^*\theta_{\xi\xi}-2\beta^*\theta_{\xi\eta}+\gamma^*\theta_{\eta\eta}=-J^2(P\theta_\xi+Q\theta_\eta)$$

Energy equation:

$$\frac{\partial T}{\partial\tau}+\frac{1}{J}\left(\frac{\partial\psi}{\partial\eta}\frac{\partial T}{\partial\xi}-\frac{\partial\psi}{\partial\xi}\frac{\partial T}{\partial\eta}\right)$$
$$=\frac{1}{J^2}\left(\alpha^*\frac{\partial^2 T}{\partial\xi^2}-2\beta^*\frac{\partial^2 T}{\partial\xi\partial\eta}+\gamma^*\frac{\partial^2 T}{\partial\eta^2}\right)$$
$$+\frac{\partial T}{\partial\xi}\left[P+\frac{1}{J}\left(\frac{2}{r}\theta_\eta-\frac{\cot\theta}{r^2}r_\eta\right)\right]$$
$$+\frac{\partial T}{\partial\eta}\left[Q-\frac{1}{J}\left(\frac{2}{r}\theta_\xi-\frac{\cot\theta}{r^2}r_\xi\right)\right] \tag{4}$$

The associated initial and boundary conditions in a calculation plane are

$$\tau=0,\quad T=0,\quad \psi=\omega=0$$
$$\tau>0$$

(a) inner sphere ($\eta=\eta_{\min}$)

$$T=0,\quad \psi=0$$
$$\omega=\frac{1}{r\sin\theta}\left[\frac{\partial^2\psi}{\partial\xi^2}\left(\frac{\partial\xi}{\partial r}\right)^2+2\frac{\partial^2\psi}{\partial\xi\partial\eta}\frac{\partial\xi}{\partial r}\frac{\partial\eta}{\partial r}+\frac{\partial^2\psi}{\partial\eta^2}\left(\frac{\partial\eta}{\partial r}\right)^2\right.$$
$$\left.+\frac{\partial\psi}{\partial\xi}\frac{\partial^2\xi}{\partial r^2}+\frac{\partial\psi}{\partial\eta}\frac{\partial^2\eta}{\partial r^2}\right] \tag{5}$$

(b) outer sphere ($\eta=\eta_{\max}$)

$$T=0,\quad \psi=0$$
$$\omega=\frac{1}{r\sin\theta}\left[\frac{\partial^2\psi}{\partial\xi^2}\left(\frac{\partial\xi}{\partial r}\right)^2+2\frac{\partial^2\psi}{\partial\xi\partial\eta}\frac{\partial\xi}{\partial r}\frac{\partial\eta}{\partial r}+\frac{\partial^2\psi}{\partial\eta^2}\left(\frac{\partial\eta}{\partial r}\right)^2\right.$$
$$\left.+\frac{\partial\psi}{\partial\xi}\frac{\partial^2\xi}{\partial r^2}+\frac{\partial\psi}{\partial\eta}\frac{\partial^2\eta}{\partial r^2}\right] \tag{6}$$

(c) upper axis line segment ($\xi=\xi_{\min}$)

$$\frac{\partial T}{\partial\xi}\frac{\partial\xi}{\partial\theta}+\frac{\partial T}{\partial\eta}\frac{\partial\eta}{\partial\theta}=0$$
$$\psi=0,\quad \omega=0 \tag{7}$$

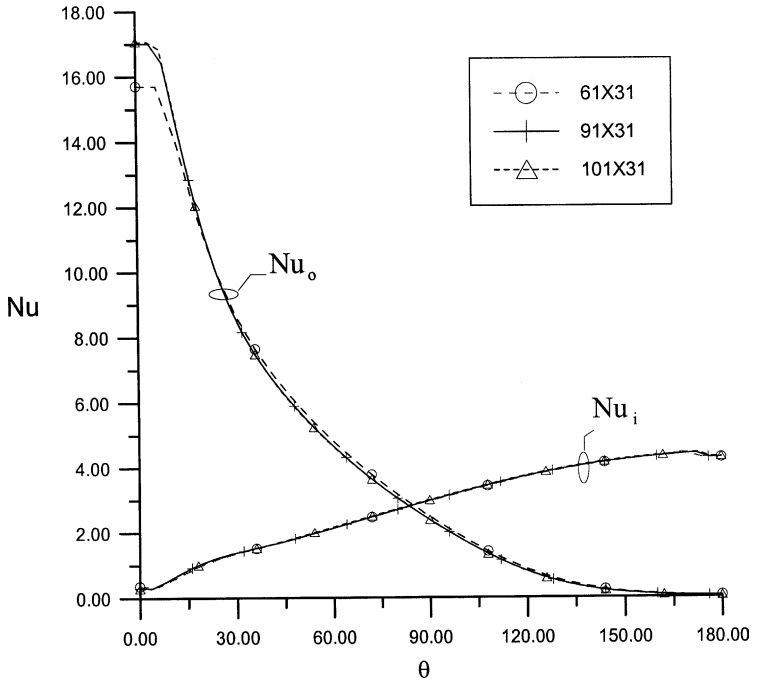

Fig. 3. Comparison of local Nusselt numbers at different grid sizes for constant viscosity ($R^* = 2.17$, $Pr = 0.7$ and $Ra = 1 \times 10^5$).

(d) lower axis line segment ($\xi = \xi_{\max}$)

$$\frac{\partial T}{\partial \xi}\frac{\partial \xi}{\partial \theta} + \frac{\partial T}{\partial \eta}\frac{\partial \eta}{\partial \theta} = 0$$
$$\psi = 0, \quad \omega = 0 \tag{8}$$

3. Numerical method

When the modified Sorenson's method [17] is used to generate the grid line, it can get the grid system with orthogonality along all boundaries and this system can enhance the accuracy of calculation. Besides, the hyperbolic tangent distribution [18] is applied to have a denser grid distribution near the boundaries. Because the weighting function scheme [19] treats with cross-derivatives effectively, we use it to discretize Eqs. (2)–(4) with the grid system. The governing equations consist of stream function equation, vorticity transport equation, and energy equation. Vorticity transport equation and energy equations are solved by employing the alternating direction implicit and stream is solved by the successive line over-relaxation method [20]. The solution was considered convergent when the relative error between the new and old values of the field variables Φ during every time step becomes less than a prescribed criterion (10^{-5}), where Φ represents T, ω and ψ.

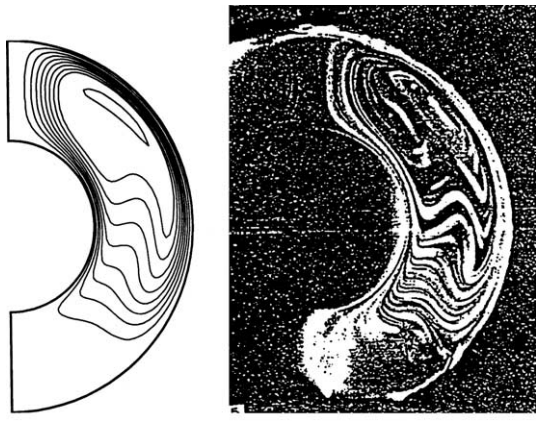

Fig. 4. A comparison of flow patterns between the present result (a) and the previous experiment (b) [19] for $R^* = 2.17$, $Pr = 0.7$ and $Ra = 7.392 \times 10^5$.

$$\frac{|\phi_{\text{new}} - \phi_{\text{old}}|_{\max}}{|\phi_{\text{new}}|_{\max}} \leqslant 10^{-5}$$

The calculated values of T, ω and ψ from above equation become the initial values of next time step, and keep replacement. Further, the convergence of the steady-state solution is determined by requiring the relative error between the present and next time step values of all

field variables for the inner and outer spheres to be within 0.001% or

$$\frac{|\phi^{n+1}-\phi^{n}|_{\max}}{|\phi^{n+1}|_{\max}} \leqslant 10^{-5}$$

The rate of heat transfer plays an important role for reference. The local Nusselt number at inner and outer radii is defined as

$$Nu_{\mathrm{i,o}} = -\frac{1}{r_{\mathrm{i}} r_{\mathrm{o}}}\left[r^{2}\frac{\partial T}{\partial r}\right]_{r=r_{\mathrm{i}},r_{\mathrm{o}}} \tag{9}$$

Table 1
Comparison of the averaged Nusselt number, the maximum stream function and vortex center position between the present result and other result for $R^{*}=2.0$, $Pr=0.7$, and $Ra=10^{3}$

	$\overline{Nu}$	$\psi_{\max}$	θ^{*} (°)
Present result	1.1025	3.249	80
Mack and Hardee [7]	1.1200	3.210	77
Atsill et al. [8]	1.1200	3.490	79
Singh and Chen [9]	1.1010	–	–
Garg [10]	1.1200	–	–
Chu and Lee [11]	1.1099	3.209	81
Chiu and Chen [12]	1.1021	3.236	81

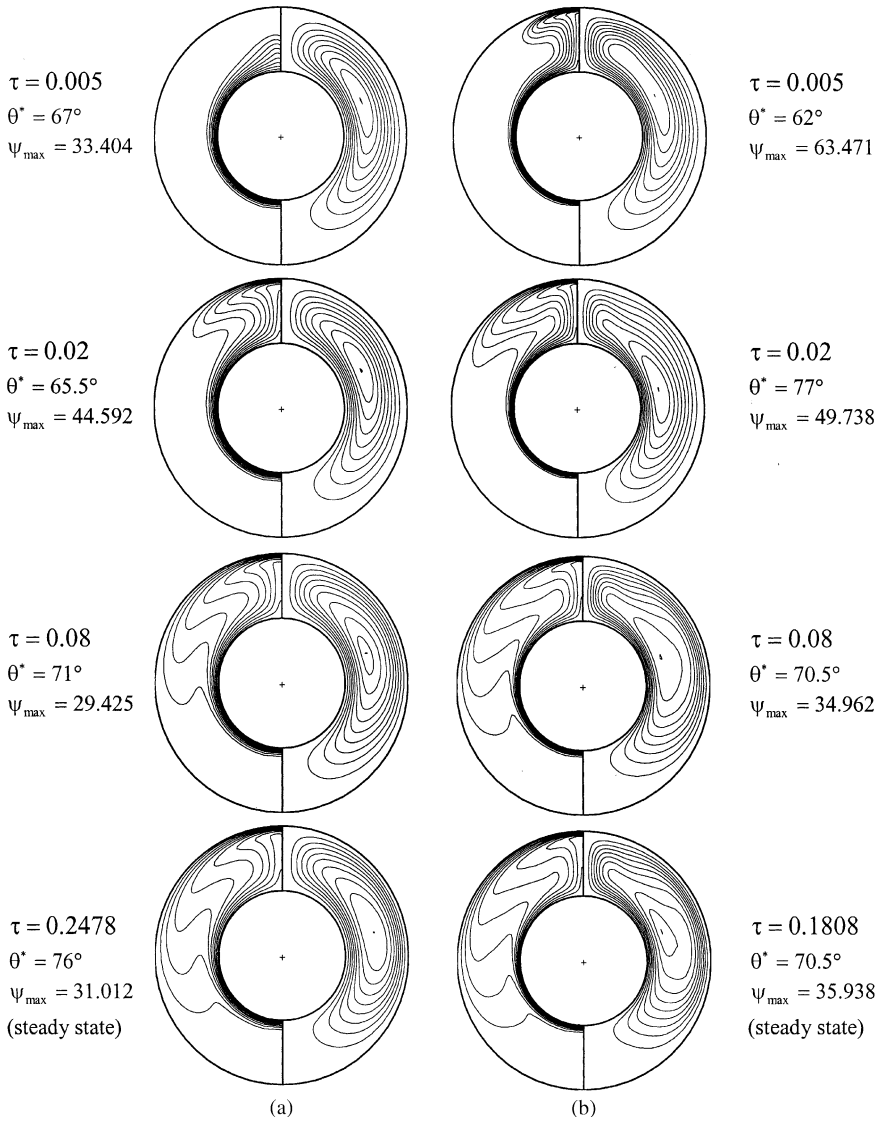

Fig. 5. Transient isotherms (left) and streamlines (right) for $R^{*}=2.0$, $Pr=405$, $Ra=6.0\times10^{4}$ and $e=0.0$ with (a) constant viscosity (b) variable viscosity.

The averaged Nusselt number at inner and outer radii is defined as

$$\overline{Nu_{i,o}} = -\int_0^x Nu_{i,o}\left[\frac{\sin(\theta)}{2}\right] d\theta \quad (10)$$

4. Results and discussion

Due to the lack of the papers on transient natural convection heat transfer of fluids with variable viscosity in a spherical annulus and between two vertically eccentric spheres, therefore, the Newtonian fluid with constant viscosity is tested at first. To check the effect of grid size on the numerical result, we used three different grid sizes to carry out the computations for a concentric annulus. Fig. 3 shows the comparison of results from three different set of grid size 61×31, 91×31, and 101×31 at Rayleigh number of 1×10^5 for a concentric annulus with constant viscous fluid at Prandtl of 0.7. From Fig. 3, the local Nusselt numbers at outer sphere for steady state have a lot much difference between 0 and 30 degrees for grid size 60×31 but the results from grid sizes 90×31 and 101×31 are very close. To make sure the accuracy of the numerical solution and time saving

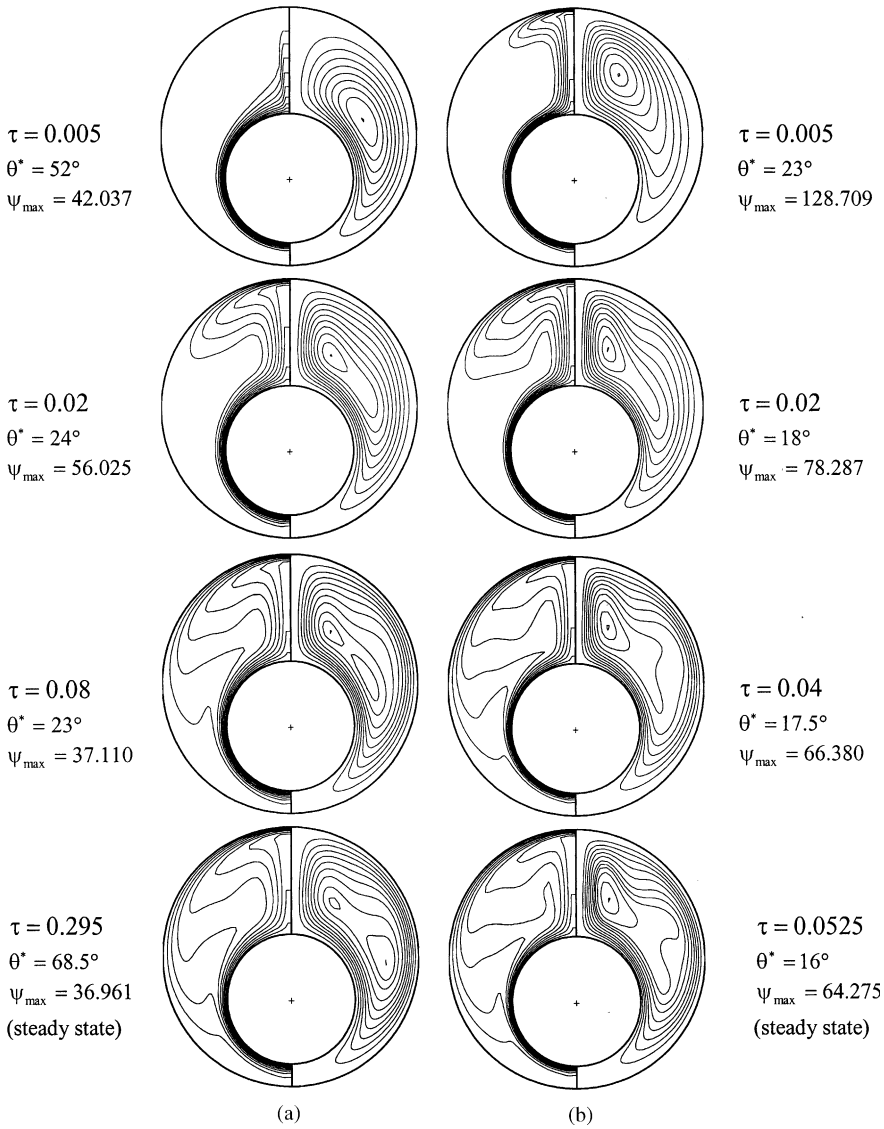

Fig. 6. Transient isotherms (left) and streamlines (right) for $R^* = 2.0$, $Pr = 405$, $Ra = 6.0\times10^4$ and $e = 0.65$ with (a) constant viscosity (b) variable viscosity.

of calculation, this article used grid size 91×31 to obtain all the results presented here. Fig. 4 shows the comparison between the calculated streamlines by the author and the measured streamlines in Yin et al. [21] for Newtonian fluid with constant viscosity. Both results are very close. Table 1 compares the calculated mean Nusselt number by the present study and by earlier papers [7–12]. The result is very accurate.

The temperature of inner sphere is higher than that of outer sphere at the initial $\tau = 0.005$ from Fig. 5(a) for fluid with constant viscosity. The fluid on outside surface of the inner sphere is heated through heat conduction from surface of inner sphere. The density of fluid becomes lower and it begins to expand. Due to the effect of gravity, the fluids close to the surface of inner sphere flow upward along the surface of the inner sphere. The hotter fluid meets on the top of inner sphere and creates a hot boundary layer next to inner sphere at this moment. At $\tau = 0.02$, since the inner sphere is kept hotter, the created upward buoyant momentum keeps whole region of fluid moving. The fluid above the top of inner sphere keeps moving upward to meet the inside surface

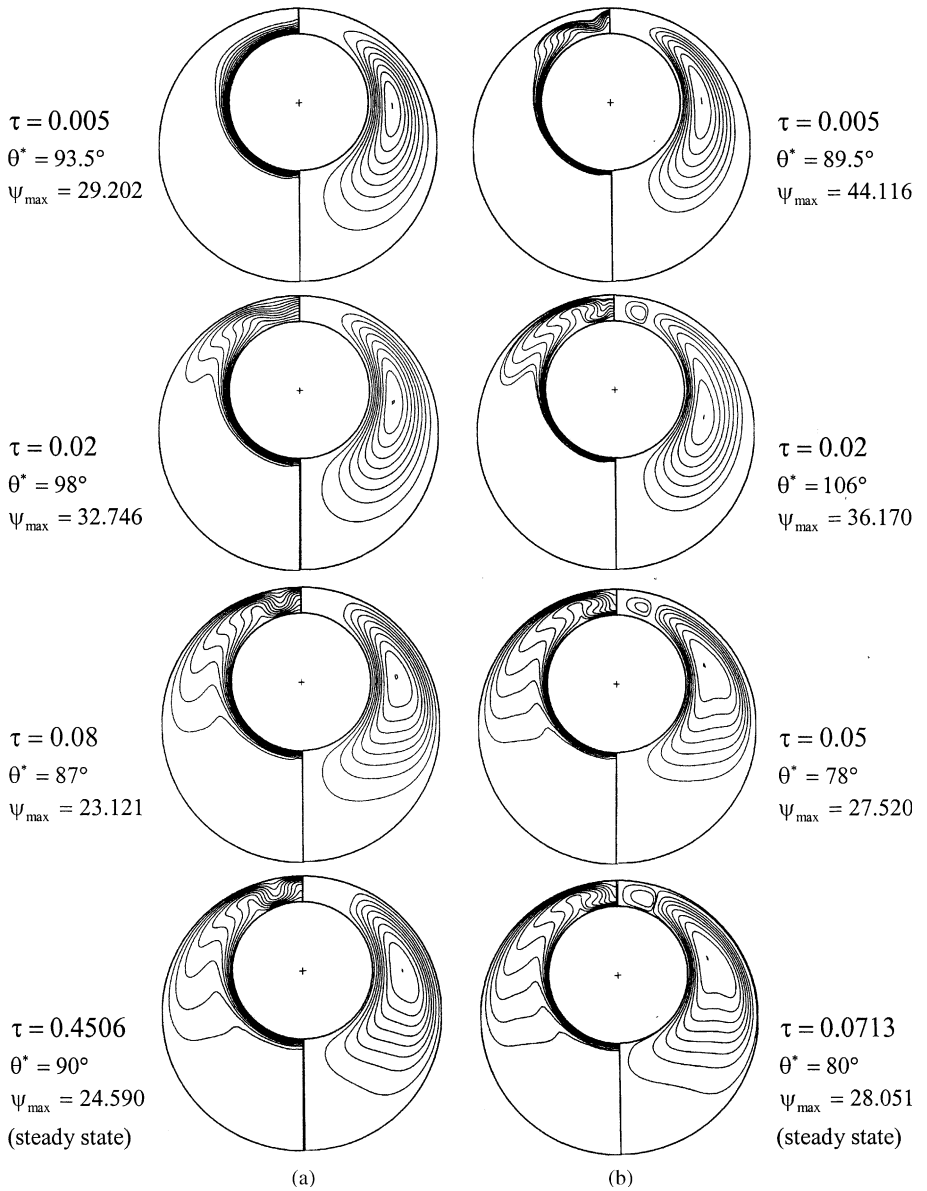

Fig. 7. Transient isotherms (left) and streamlines (right) for $R^* = 2.0$, $Pr = 405$, $Ra = 6.0 \times 10^4$ and $e = -0.65$ with (a) constant viscosity (b) variable viscosity.

of outer sphere. The temperature of outer sphere is lower, and due to the action of convective heat transfer from fluid, the heat transfers outside the wall of outer sphere. The fluid on inside surface of the outer sphere is cooled and the density of fluid becomes higher. The fluids close to the surface of outer sphere flow downward along the surface of the outer sphere due to the effect of buoyancy. It forms a shape like a feather-column and the shape is named as Thermal Plume. Until $\tau = 0.08$, the downward fluid close to outer sphere forms a cold boundary layer next to outer sphere. At last steady state and $\tau = 0.2478$, the fluid reaches the bottom surface of outer sphere and do not rise any more. It forms a stagnation area and shows a moving enclosed ring of fluid. This is displayed on the streamline distribution. Fig. 5(b) shows that the development of temperature field for the fluid with variable viscosity is the same as the fluid with constant viscosity at the same condition, but the distortion on isotherm distribution is more obvious than the fluid with constant viscosity. The vortex center represents the maximum value of stream function. The value of the vortex center is 44.592 at $\tau = 0.02$ from Fig. 5(a), but that of the vortex center is 63.471 at $\tau = 0.005$ from Fig. 5(b). The variation of streamline in the fluid with variable viscosity is larger than the fluid with constant viscosity and it reaches the maximum value faster. This proves that the effect of buoyancy in the fluid with variable viscosity is stronger, the development of its isotherm is distorted earlier and finally it reaches steady state faster than the fluid with constant viscosity.

From Fig. 6 for the fluids with variable viscosity and constant viscosity, the change of isotherms in two vertically eccentric spheres with the eccentricity of 0.65 is similar to the development in a spherical annulus. The change of eddy following the thermal plume begins development. The vortex center rises rapidly and the thermal plume moves downward along the interior of outer sphere. After reaching the steady state, the vortex center in fluid with constant viscosity is located at

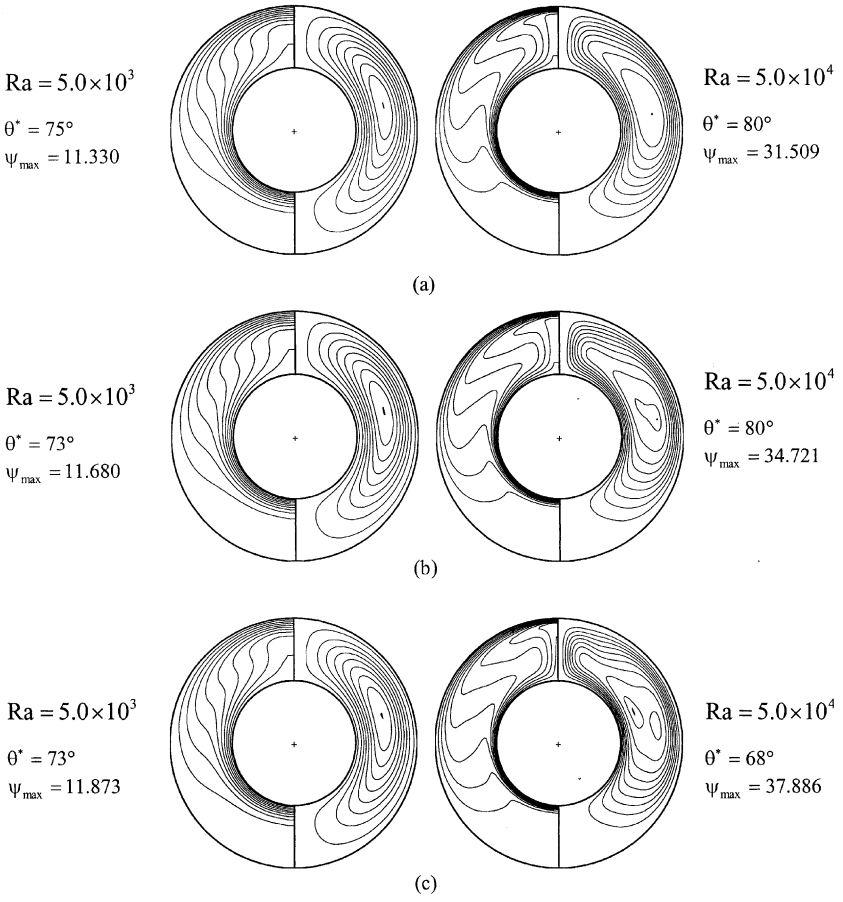

Fig. 8. Steady isotherms (left) and streamlines (right) for $R^* = 2.0$, $e = 0.0$, and different Rayleigh numbers with variable viscosity (a) $Pr = 158$, (b) $Pr = 405$, (c) $Pr = 720$.

around $\theta^* = 68.5°$ steadily, and the vortex center in fluid with variable viscosity is located at around $\theta^* = 18.5°$. The value of streamline function in the fluid with variable viscosity is larger than the fluid with constant viscosity and both values are larger than those in the spherical annulus. This specifies that the outer sphere has a bigger heat absorbing area; therefore positive eccentricity configuration has a better effect of convection heat transfer. The definition of critical Rayleigh number (Ra_c) represents the critical value of Rayleigh number for the transition of elementary flow regime to secondary Flow regime, but the primary vortex center is located above the inner sphere as shown in Fig. 6(a). The streamlines collapse from original unicellular convection vortex into two convection vortexes. The newly formed vortex is named as secondary vortex and this is secondary flow regime. For negative eccentricity configuration in Fig. 7 and the fluids with variable viscosity and constant viscosity, the heat absorbing area above inner sphere is smaller and has the disadvantage to the method of natural convection heat transfer. The method of conduction is the main governing mechanism of heat

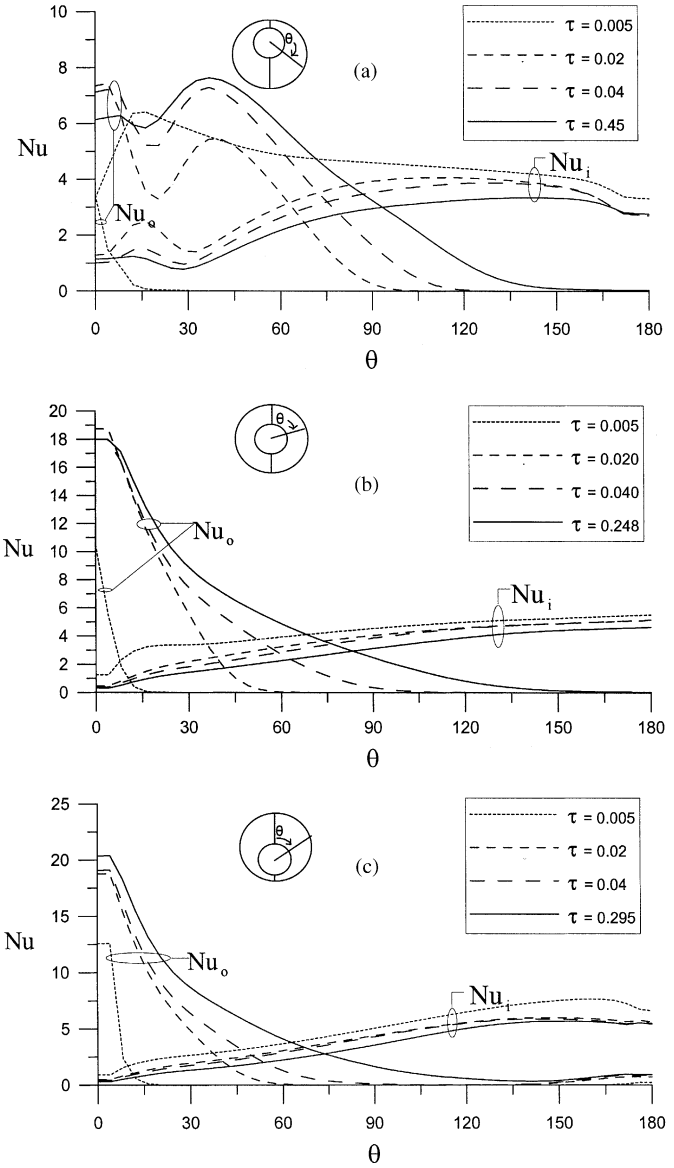

Fig. 9. Transient variation of local Nusselt number for constant viscosity with $R^* = 2.0$, $Pr = 405$ and $Ra = 6 \times 10^4$ (a) $e = -0.65$, (b) $e = 0.0$, (c) $e = 0.65$.

transfer in the upper portion of inner sphere. For the fluid with variable viscosity, a counter-clockwise secondary streamline nest displays above the inner sphere at $\tau = 0.02$ and its value of streamline is -34.137. Therefore, it makes the isotherms display a phenomenon of severe distortion. The value of streamline is -2.68 in secondary streamline nest at the steady state. In this situation, it is similar to that Caltagirone et al. [22] have stated. In general, the secondary streamline nest occurs at the condition of critical Rayleigh number. This specifies that the fluid with variable viscosity reaches to the critical Rayleigh number faster than the fluid with constant viscosity. From the fluids with variable viscosity and constant viscosity in both spherical annulus and between two vertically eccentric spheres, the higher the location of vortex center above inner sphere is at steady state, the stronger the effect of convection is and the larger the value of streamline is.

Fig. 8 is a comparison of isotherms and streamlines at the steady state when the Rayleigh number and Prandtl number change for the fluid with variable viscosity. The value of streamlines becomes larger as the value of

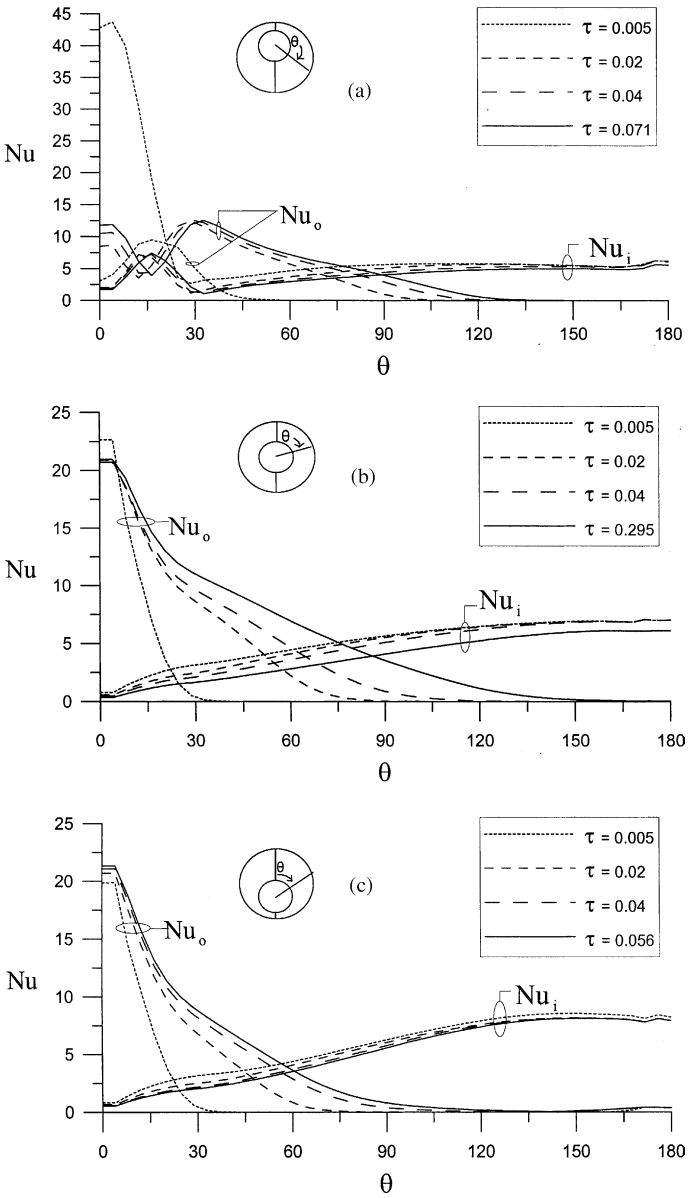

Fig. 10. Transient variation of local Nusselt number for variable viscosity with $R^* = 2.0$, $Pr = 405$ and $Ra = 6 \times 10^4$ (a) $e = -0.65$, (b) $e = 0.0$, (c) $e = 0.65$.

Ra becomes larger from. This specifies that the effect of buoyancy becomes larger as *Ra* increases, and thus it enhances the effect of convection heat transfer. When Rayleigh number is 5.0×10^3, the developments on both isotherms and streamlines in Fig. 8 are almost the same. At $Ra = 5.0\times10^4$, the value of streamline for $Pr = 720$ is larger than those for $Pr = 158$ and $Pr = 405$. This proves that the fluid with variable viscosity and high Prandtl number can enhance the effect of buoyancy and it is more distinct as Rayleigh number becomes larger. As shown in Fig. 8(c) $Pr = 720$, it has reached to the state of secondary vortex. Fig. 8(a) $Pr = 158$ and Fig. 8(b) $Pr = 405$ with same Rayleigh number show that the phenomenon does not occur yet. This specifies that as *Pr* is increased, the concentration of glycerol–water solutions will increase, and then the effect of thermal convection is stronger, and the critical Rayleigh number will be decreased.

Figs. 9 and 10 are the distributions of transient local Nusselt numbers contrast to Figs. 5–7 related to angular position. In Figs. 9(b) and (c) and 10(b) and (c), the distributions of local Nusselt numbers Nu_o on the interior of outer sphere are the minimums at the beginning and then reach to the whole maximums at steady state. The distributions of local Nusselt numbers Nu_i on the exterior of inner sphere are the maximums at the

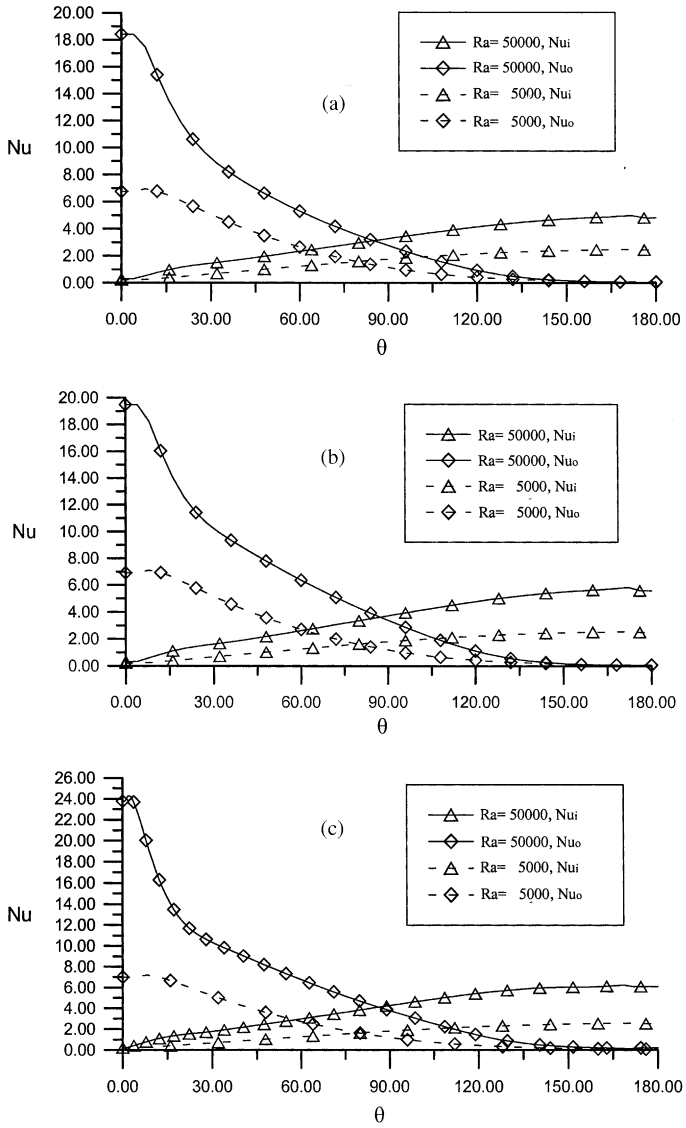

Fig. 11. Steady local Nusselt number versus angle position at $R^* = 2.0$, $Ra = 5.0\times10^3$ and 5.0×10^4 for fluid with variable viscosity (a) $Pr = 158$, (b) $Pr = 405$, (c) $Pr = 720$.

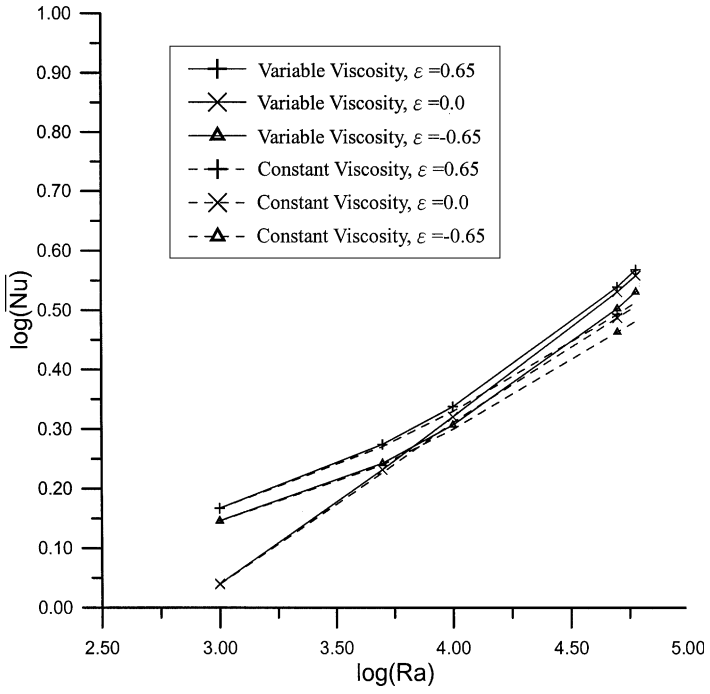

Fig. 12. Relation of averaged Nusselt number ($\overline{Nu}$) with Rayleigh number (Ra) at steady state for $R^* = 2.0$ and $Pr = 158$.

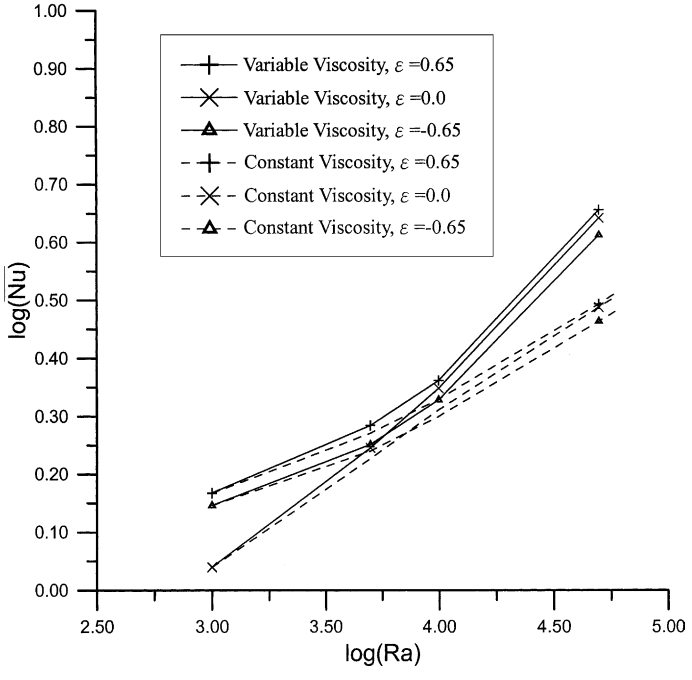

Fig. 13. Relation of averaged Nusselt number ($\overline{Nu}$) with Rayleigh number (Ra) at steady state for $R^* = 2.0$ and $Pr = 720$.

beginning and then reach to the whole minimums at steady state; the local Nusselt numbers Nu_i are the minimums at $\theta^* = 0°$. The local Nusselt numbers Nu_o on the interior of outer sphere are the maximums at steady

Table 2
Averaged Nusselt number with Rayleigh number and eccentricity of glycerol–water solution with constant viscosity

ε	Ra					
	1.0×10^3	5.0×10^3	1.0×10^4	5.0×10^4	6.0×10^4	6.5×10^4
$\overline{Nu}$ *for* $Pr = 405$						
0.65	1.4685	1.8650	2.1355	3.1135	3.2635	3.3320
0.0	1.0946	1.6850	2.0460	3.0605	3.1975	3.2795
−0.65	1.3985	1.7360	1.9925	2.8965	3.0345	3.0955
$\overline{Nu}$ *for* $Pr = 158$						
0.65	1.4684	1.8648	2.1360	3.1140	3.2645	–
0.0	1.0946	1.6853	2.0463	3.0722	3.2149	–
−0.65	1.3985	1.7365	1.9930	2.9071	3.0321	–
$\overline{Nu}$ *for* $Pr = 720$						
0.65	1.4685	1.8649	2.1355	3.1132	3.2636	–
0.0	1.0946	1.6853	2.0464	3.0726	3.2149	–
−0.65	1.3985	1.7365	1.9930	2.9071	3.0347	–

Table 3
Averaged Nusselt number of glycerol–water solution with variable viscosity

ε	Ra					
	1.0×10^3	5.0×10^3	1.0×10^4	5.0×10^4	6.0×10^4	6.5×10^4
$\overline{Nu}$ *for* $Pr = 405$						
0.8	1.8476	2.2450	2.5517	4.1756	–	–
0.65	1.4726	1.9055	2.2435	4.0150	4.3900	4.5725
0.0	1.0988	1.7385	2.1675	3.9135	4.2555	4.4220
−0.65	1.4009	1.7690	2.0825	3.6610	4.0100	4.2440
−0.8	1.7652	2.0825	2.3466	3.6526	–	–
$\overline{Nu}$ *for* $Pr = 158$						
0.65	1.4691	1.8803	2.1758	3.4622	3.7030	–
0.0	1.0963	1.7055	2.0921	3.3967	3.6193	–
−0.65	1.3995	1.7490	2.0265	3.1852	3.3985	–
$\overline{Nu}$ *for* $Pr = 720$						
0.65	1.4709	1.9231	2.2994	4.5313	–	–
0.0	1.0966	1.7596	2.2296	4.3865	–	–
−0.65	1.3994	1.7824	2.1288	4.0997	–	–

state and $\theta^* = 0°$. Nu_o and Nu_i have the maximums and the minimums in the fluid with constant viscosity in Fig. 9(a), but the maximums and minimums are always at $\theta^* = 0$–$45°$ as time proceeds. This shows that secondary vortex can occur. The maximums of Nu_o in the fluid with variable viscosity in Fig. 9(b) are between 25° and 30° all the time, and therefore secondary vortex displays at $\theta^* = 25°$ and steady state. The negative eccentricity configuration generates the disadvantageous condition for natural convection; this makes maximums of Nu_o and Nu_i less than those in both spherical annulus and positive eccentric spheres.

Fig. 11(a)–(c) are the distributions of steady local Nusselt numbers related to angular position when Prandtl number changes. The effect of different Rayleigh number on result of heat transfer can be seen. According to the condition $Pr = 158$ in Fig. 11(a), the local Nusselt numbers on exterior of inner sphere have minimums at $\theta^* = 0°$. The value of Nu_i increases as angular degree increases; the maximums occur at $\theta^* = 180°$. The whole variation is not large due to the formation of heat boundary layer on exterior of inner sphere. Except at $\theta^* = 0°$, the variation of thickness is smaller than that of the rest due to the rising upward of fluid, so that the coefficient of heat transfer has not much variation. The local Nusselt numbers on interior of outer sphere (Nu_o) decrease gradually as angular degree increases. The minimums are located at $\theta^* = 180°$. The whole variation is larger than Nu_i because the thickness of heat boundary layer on interior of outer sphere is very thin and the

coefficient of heat transfer is larger. Nu_o decreases because the heat boundary layer becomes thicker as it moves downward and generates stagnation area at the bottom of outer sphere; the coefficient of heat transfer is smaller. Therefore, the values of Nu_o have big variation with angular position. From a comparison of Fig. 11(a) with (b) and (c), the effect of variable viscosity at $Ra = 5 \times 10^3$ does not affect the Nusselt number distributions too much even with different Prandtl numbers; the values of Nu_i or Nu_o almost have similar trend. Until $Ra = 5 \times 10^4$, Nu_i or Nu_o of fluid with variable viscosity for $Pr = 720$ is larger than Nu_i or Nu_o of fluid with variable viscosity for $Pr = 158$ and 405 and the maximum values are larger.

For $Pr = 158$ and 720 in Figs. 12 and 13 and, the corresponding average Nusselt numbers are also plotted versus the Rayleigh numbers in a logarithmic–logarithmic coordinates. The higher the Prandtl number is, the larger the Nu is for the same Ra number. The Nusselt numbers and Ra number in a logarithmic–logarithmic coordinates are linear related in laminar flow regime. The related equation is

$$\overline{Nu} = CRa^m \tag{11}$$

The average Nusselt numbers are obtained from Tables 2–5. They represent the average value of heat transfer from the viewpoint of engineering and an investigation of the important effect of the integral average value of heat transfer in different Ra number. That the average value of heat transfer increases as Ra number increases regardless of fluids with constant or variable viscosity. C and exponent m of Eq. (11) are listed in Tables 2–5 for three individual fluids with different Prandtl number and constant viscosity or variable viscosity in a spherical annulus and between two vertically eccentric spheres. The maximum error is less than 5%.

Table 4
The coefficient of Eq. (9) of glycerol–water solution with constant viscosity

ε	C	m	Ra
$Pr = 405$			
0.65	0.3472	0.2022	1.0×10^3–6.5×10^4
0.0	0.1816	0.2613	1.0×10^3–6.5×10^4
−0.65	0.3394	0.1975	1.0×10^3–6.5×10^4
$Pr = 158$			
0.65	0.3559	0.1991	1.0×10^3–6.0×10^4
0.0	0.1794	0.2628	1.0×10^3–6.0×10^4
−0.65	0.3478	0.1944	1.0×10^3–6.0×10^4
$Pr = 720$			
0.65	0.3560	0.1991	1.0×10^3–6.0×10^4
0.0	0.1794	0.2628	1.0×10^3–6.0×10^4
−0.65	0.3475	0.1946	1.0×10^3–6.0×10^4

Table 5
The coefficient of Eq. (9) of glycerol–water solution with variable viscosity

ε	C	m	Ra
$Pr = 405$			
0.8	0.0332	1.8494	1.0×10^3–5.0×10^4
0.65	0.1864	0.2834	1.0×10^3–6.5×10^4
0.0	0.1018	0.3376	1.0×10^3–6.5×10^4
−0.65	0.1862	0.2756	1.0×10^3–6.5×10^4
−0.8	0.0319	1.8098	1.0×10^3–5.0×10^4
$Pr = 158$			
0.65	0.2786	0.2311	1.0×10^3–6.0×10^4
0.0	0.1434	0.2924	1.0×10^3–6.0×10^4
−0.65	0.2802	0.2227	1.0×10^3–6.0×10^4
$Pr = 720$			
0.65	0.1835	0.2867	1.0×10^3–5.0×10^4
0.0	0.0904	0.3540	1.0×10^3–5.0×10^4
−0.65	0.1901	0.2742	1.0×10^3–5.0×10^4

5. Conclusion

The effects of variable viscosity on transient flow field, temperature distribution and Nusselt number have been investigated for the natural convection between two concentric (and vertically eccentric) spheres. The numerical obtained results further indicated that heat and flow patterns vary with the Rayleigh number and the eccentricity of the annulus under various Prandtl numbers. The Prandtl number does not affect the flow field for lower Ra number. When Ra number increases, the higher the Prandtl number is, the less stable the flow field is, and it reaches critical state earlier. At $Ra > Ra_c$, elementary flow field loses its stability and is transformed into secondary flow regime. Ra_c decreases as Prandtl number increase. The effect of variable viscosity enhances the result of convection and increases rate of heat transfer. The characteristic of heat transfer from flow field can be expressed as a linear relation of log of Nu and log of Ra under various Prandtl numbers. The positive eccentric configuration can obtain better result of heat transfer but the negative eccentric configuration has disadvantageous space for the development of natural convection and decreases the result of heat transfer.

Acknowledgements

The authors gratefully acknowledge the financial support for this project by the National Science Council of the Republic of China.

References

[1] B. Gebhart, Y. Jaluria, R.L. Mahajan, B. Sammaia, Buoyancy-Induced Flows and Transport, Hemisphere, Washington, DC, 1985, pp. 725–816.

[2] R.N. Horne, M.J. O'Sullivan, Convection in a porous medium heated from below: the effect of temperature dependent viscosity and thermal expansion coefficient, J. Heat Transfer 100 (1978) 448–452.
[3] A.R. Wazzan, T.T. Okamura, A.M.O. Smith, The stability of water flow over heated and cooled flat planes, J. Heat Transfer 90 (1968) 109–114.
[4] A.R. Wazzan, T.T. Okamura, A.M.O. Smith, The stability and transition of heated and cooled incompressible laminar boundary layers, in: Proceedings of the Fourth International Heat Transfer Conference, Paris, 1970.
[5] J.Y. Jang, J.C. Mollendorf, The Stability of a vertical natural convection boundary layer with temperature dependent viscosity, Int. J. Eng. Sci. 26 (1988) 1–12.
[6] H.M. Chou, J.N. Chuang, W.C. Tsai, I.H. Lin, Studies on natural convection of variable viscosity fluids between concentric and eccentric horizontal cylindrical annuli, in: The 26th Conference on Theoretical and Applied mechanics, Yulin, Taiwan, December 2002.
[7] L.R. Mack, H.C. Hardee, Natural convection between concentric spheres at low Rayleigh numbers, Int. J. Heat Mass Transfer 11 (1968) 387–396.
[8] K.N. Astill, H. Leong, R. Martorana, A numerical solution for natural convection in concentric spherical annuli, in: Proceedings of the 19th National Heat Transfer Conference, ASME HTD, vol. 8, 1980, pp. 105–113.
[9] S.N. Singh, J. Chen, Numerical solution for free convection between concentric spheres at moderate Grashof numbers, Numer. Heat Transfer 3 (1980) 441–459.
[10] V.K. Garg, Natural convection between concentric spheres, Int. J. Heat Mass Transfer 35 (1992) 1935–1945.
[11] H.S. Chu, T.S. Lee, Transient natural convection heat transfer between concentric spheres, Int. J. Heat Mass Transfer 36 (1993) 3159–3170.
[12] C.P. Chiu, W.R. Chen, Transient natural convection heat transfer between concentric and vertically eccentric sphere, Int. J. Heat Transfer 39 (7) (1996) 1439–1452.
[13] T.S. Lee, G.S. Hu, C. Shu, Application of GDQ method for the study of natural convection in horizontal eccentric annuli, Numer. Heat Transfer 8 (2002) 803–815.
[14] Y.M. Chen, A.J. Pearlstein, Viscosity–temperature correlation for glycerol–water solutions, Ind. Eng. Chem. Res. 26 (1987) 1670–1672.
[15] J.B. Segur, Physical properties of glycerol and its solutions, in: C.S. Miner, N.N. Dalton (Eds.), Glycerol, Reinhold, 1953, pp. 238–334.
[16] J.B. Segur, H.E. Oberstar, Viscosity of glycerol and its aqueous solutions, Ind. Eng. Chem. 43 (1952) 117–21201.
[17] R.L. Sorenson, Three-dimensional elliptic grid generation about fighter aircraft for zonal finite-difference computations, AIAA Paper no. 86-0429, New York, 1986.
[18] M. Vinokur, On one-dimensional stretching functions for finite-difference calculations, J. Comput. Phys. 50 (1983) 215–234.
[19] S.L. Lee, T.S. Chen, B.F. Aramaly, New finite difference solution methods for wave instability problem, Numer. Heat Transfer 10 (1986) 1–18.
[20] P.R. Roache, Computational Fluid Dynamics, Hermosa Publishers, 1972, pp. 91–95, 117–119.
[21] S.H. Yin, R.E. Powe, J.A. Scanlan, E.H. Bishop, Natural convection flow patterns in spherical annuli, Int. J. Heat Mass Transfer 16 (1973) 1785–1795.
[22] J.P. Caltagirone, M. Combarnous, A. Mojtabi, Natural convection between two concentric spheres: transition toward a multi-cellular flow, Numer. Heat Transfer 3 (1980) 107–739.